Spectrum redshift effect of anatase TiO_2 codoped with nitrogen and first transition elements

Yonghong Gu (辜永红)[1,2], Congzhong Cai (蔡从中)[1], Qing Feng (冯 庆)[2*], and Yanhua Li (李艳华)[1]

[1]*Department of Applied Physics, Chongqing University, Chongqing 401331, China*
[2]*Chongqing Key Laboratory on Optoelectronic Functional Materials, Chongqing Normal University, Chongqing 401331, China*
[*]*Corresponding author: fengq_126@163.com*

Received April 14, 2014; accepted May 20, 2014; posted online August 28, 2014

The electronic and optical properties, including band structure, density of states (DOS), absorption rate, refractive index, and dielectric function, of anatase TiO_2 codoped with N and first transition elements are investigated using the plane wave pseudopotential method based on the density functional theory. The calculation results show that TiO_2 codoping with N and first transition elements (Sc, V, Cr, Mn, and Fe) lead to significant reduction of conduction band relative to the Fermi level, reduction of band gap width, formation of new donor, and acceptor impurity levels below the conduction band and above the valence band, and cause some redshifts of optical absorption band edge with the amount of redshift decrease in the following order: N–Fe > N–Cr > N–Mn. Further, the synergistic effect of shallow donor and acceptor levels enhances light excitation for effective separation of electron–hole pairs and enhancement of light absorption ability, thereby increasing the TiO_2 photocatalytic properties. This study reveals that the visible-light absorption ability of the codoped anatase TiO_2 decreases in the order of N–Fe > N–Cr > N–Mn > N–Sc > N–V > N, and does not monotonically follow the dopant atomic number. Especially, in N–Cr codoped TiO_2, the 4s atomic orbit of Cr is not completely filled, which hybridized with the p electronic orbit most probably acts as photo-generated electron trap centers resulting in higher photocatalytic activity than that of N–Mn codoped TiO_2.

OCIS codes: 160.6990, 160.4760.
doi: 10.3788/COL201412.091602.

In 1972, Fujishima *et al.* discovered the photocatalytic effect of TiO_2 when they conducted the single-crystal electrode water decomposition experiment[1]. Under normal temperature and pressure, TiO_2 has three polymorphs: rutile, anatase, and brookite. The optical performance of anatase TiO_2 is superior to other materials[2] because of its high photocatalytic ability, photoelectric conversion efficiency, hydroxylation, and oxygen adsorption capacity. However, the band gap of anatase TiO_2 is approximately 3.23 eV. It can exhibit good catalytic activity only in the ultraviolet band, and its rate of utilization of solar energy is low. Therefore, effective improvement of anatase TiO_2 response to visible (VIS) light and solar energy utilization are the important concerns of this widely used photocatalytic material[3–8].

In 2001, Asahi *et al.*[9] conducted a photocatalytic activity experiment on N-doped TiO_2. The results showed that the doped N can improve the photocatalytic activity of TiO_2 in different degrees. Since then there has been increasing interest in nonmetal doping of TiO_2 to improve its photocatalytic ability. It's found that the photocatalytic activity of TiO_2 can be improved by doping with most of the transition metal elements in the periodic table such as Fe^{3+}, Ru^{3+}, and Os^{3+}, and its photocatalytic activity can be reduced by doping with Li^+, Mg^{2+}, Al^{3+}, Ga^{3+}, etc[10]. Further, Umebayashi *et al.*[11] studied the electronic structure of 3d transition metal-doped anatase TiO_2 using the linear augmented plane wave method is studied based on the density functional theory[11]. It's found that the d electrons in the t_{2g} orbital produce an impurity level in the forbidden or valence band, and the impurity level shifts to lower energy levels as the electronegativity of the impurity increases. The optical properties of 3d transition metal-doped anatase TiO_2 is studied[12]. It's found that the doping position in the band gap is an important factor affecting the redshift of TiO_2 absorption edges.

However, theoretical analysis is not sufficient to improve the TiO_2 optical properties through codoping TiO_2 with nonmetallic elements and transition metals to improve the synergy between donor and acceptor impurities on TiO_2. Therefore, the band structure, density of states (DOS), and optical properties of the nonmetallic element N and transition metals (Sc, V, Cr, Mn, and Fe) codoped TiO_2 are investigated using the plane wave pseudopotential method, which is based on the density functional theory. We systematically analyze the relationship of different transition elements such as Sc, V, Cr, Mn, and Fe between the 3d electronic arrangement and the electronic band structure. Further, a comparative study on the effect of codoping TiO_2 with different transition elements on the optical properties of anatase TiO_2 is presented. Above all, we

want to provide theoretical references for experimental research on improving the photocatalytic properties of anatase TiO_2.

Anatase TiO_2 belongs to the tetragonal crystal system. The space group is $I4_1/amd$, and its vector lattice contains eight O atoms and four Ti atoms. Further, considering computing power and actual situation, a supercell model comprising four $(2\times3\times1)$ original cells (Fig. 1(a)) is analyzed in this study. After doping, the distance between the metal impurities and the nonmetallic element N is greater than 1 nm. We can ignore the interaction between impurity atoms. The molecular formula is $Ti_{24}O_{48}$. Because of the periodic crystal symmetry, the apex angle and the edge are 1/8th and 1/4th of the atom, respectively, whereas the surface is 1/2th of the atom.

We constructed a $2\times3\times1$ supercell model of N and N–A (A = Sc, V, Cr, Mn, Fe) codoped TiO_2. An O atom is replaced by N atom, and a Ti atom is replaced by Sc, V, Cr, Mn, or Fe atoms (Figs. 1(b) and (c)).

The CASTEP[13] software package, which is based on the density functional theory, is employed for calculations. In addition, the ultra-soft pseudopotentials that can reduce the number of plane waves are used to describe the interaction between electrons and ions. Further, the PBESOL[14] program of the generalized gradient approximation (GGA) is used to describe the exchange-correlation energy of the interaction between electrons. The plane wave cutoff energy is considered to be 340 eV. We calculate the first Brillouin zone using the Monkhorst–Pack program in the reciprocal space of k. We select $3\times5\times2$ separate compartments. First, the lattice model of nonmetallic element N and N–A (A = Sc, V, Cr, Mn, Fe) codoped pure anatase TiO_2 is established. Subsequently, we perform structural optimization. The convergence accuracy is 2×10^{-5} eV, and internal stress is less than 0.05 GPa. Further, the maximum stress of every atom is less than 0.03 eV/nm. We calculate the band structure of the crystal model, the total DOS (TDOS), partial DOS (PDOS), and optical properties (such as dielectric constant, absorptivity, and reflectivity). The valence electrons that are involved in calculation are O $2s^22p^4$, N $2s^22p^3$, Sc $3d^14s^2$, V $3d^34s^2$, Cr $3d^54s^1$, Mn $3d^54s^2$, Fe $3d^64s^2$, and Ti $3d^24s^2$.

First, the structure of the crystal cell of pure anatase TiO_2 is optimized. Subsequently, the lattice constant is determined. A comparison of the experimental[15] and theoretical[16] lattice constant values is shown in Table 1. We use the PBESOL program of the GGA. The unit cell parameters are $a = 0.3766$ nm, $c = 0.9486$ nm, and $u = 0.207$. The deviation is minimal when compared with other approximate program. The differences between the experimental and obtained values are 0.42%, 0.16%, and 0.48%, proving the validity of this method.

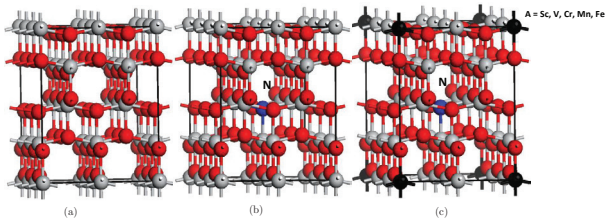

Fig. 1. $2\times3\times1$ supercell structures of (a) TiO_2, (b) $TiNyO_{2-y}$, and (c) $Ti_{1-x}A_xN_yO_{2-y}$. A = Sc, V, Cr, Mn, Fe.

The band structure of pure anatase TiO_2 is shown in Fig. 2(a). The minimum band gap is calculated to be 2.134 eV, which is less than the experimental value of 3.23 eV. However, when compared with the calculation results (2.0 eV) in Ref. [9], it is closer to the experimental value. Nevertheless, a large deviation exists between the calculation and experimental semiconductor band gap values[17–30]. This underestimation of band gap values by calculation can be attributed to the use of density functional theory to handle exchange-correlation energy in which the electric density is applied near one reference point; thus, the multi-electron interaction energy is not fully described. Therefore, we need scissors operator correction, and the correction value is 1.096 eV.

The band structure of the doped system is shown in Fig. 2. After codoping TiO_2 with N and N–A (A = Sc, Cr, Mn, Fe), the conduction and valence bands shift relatively closer to the Fermi level. Irrespective of the impurity level, the width of the forbidden band decreases relative to the band gap of pure anatase TiO_2. Four impurity levels are formed in the forbidden band in the N–Cr codoped TiO_2 (Fig. 2(e)). They are approximately 0.416 eV from the bottom of the conduction band to the highest point of the donor impurity level, and approximately 1.133 eV from the top of the valence band to the lowest point of the acceptor impurity level. The width of the forbidden band is reduced to 2.192 eV. The Fermi energy level is in the gap of impurity level. Electrons may transit from the valence band to the acceptor impurity level or from the donor impurity level to the conduction band. Consequently, the response to VIS light can be significantly improved. The conduction band is clearly shifted below the Fermi level when TiO_2 is codoped with N–Mn or N–Fe (Figs. 2(f) and (g)). The bottom of the conduction band is at 1.763 and 1.839 eV, respectively. The widths of the forbidden bands are reduced to 2.255 and 2.23 eV, respectively. Meanwhile, the donor and acceptor impurity levels are formed at the bottom of the conduction band and above the valence band. Electrons can transit from the valence band to the impurity level or from impurity level to the conduction band. In conclusion, for the N–A (A = Sc, V, Cr, Mn, Fe) codoped TiO_2, the synergistic effect between the donor level and the acceptor level can improve the photocatalytic activity of TiO_2 in the VIS region. From a comparison of the band structures of different doping systems, we can see that multiple impurity levels are formed in the forbidden band when TiO_2 is codoped with N–Fe, N–Mn, or N–Cr. Moreover, the width of

Table 1. Comparison of Experimental and Theoretical Anatase TiO_2 Lattice Constants

		Theory		This study	
	Experiment	**Results**	**Deviation(%)**	**Results**	**Deviation(%)**
a (nm)	0.3782	0.3692	−2.37	0.3766	−0.42
c (nm)	0.9502	0.9471	−0.33	0.9486	−0.16
c/a	2.512	2.566	2.14	2.519	0.70
u	0.208	0.206	−0.96	0.207	−0.48

the forbidden band decreases in accordance with the band gap of pure anatase TiO_2. For N-doped or N–Sc codoped TiO_2, only one impurity level is formed in the forbidden band. After codoping TiO_2 with N–V, four impurity levels are formed, but the width of the forbidden band increases to 3.273 eV. From the band structure of N–Cr, N–Mn, and N–Fe, it can be found that the Fermi level goes through some impurity band, which seems to make the codoped system presenting some characteristics of metal. By comparison with pure metals, the metallicity of the codoped system does not appear too strong. One reason is that the doping concentration is at very low levels in practice to bring little free charge carriers. Another reason can be found in Fig. 3 that the TDOSs of the three codoped system are significantly different from those of pure metals. Generally, near the Fermi level pure metal has a high DOS. However, the TDOSs of the three codoped systems are much smaller than that of pure metal. Although the band is half full, the codoped system still exhibits semiconductor characteristics for it contains less free charge carriers. In addition, although the recombination might have occurred between a certain amount of photogenerated electrons and photogenerated holes, the excitation photon energies would be dropped much more and the number of photogenerated electrons is also greater than other codoped system for the reasons of the band gap decreasing and impurity level emerging, which would cause the number of electrons excited to the conduction band increase. Therefore, from the comparative analysis of the band structure, we know that the photocatalytic activity of TiO_2 increases in the VIS region when it is codoped with N–Fe, N–Mn, or N–Cr as opposed to N–Sc or N–V.

The TDOS varies when TiO_2 is doped with N or codoped with N–A (A = Sc, V, Cr, Mn, Fe), as shown in Fig. 3.

Both the top of the valence band and the bottom of the conduction band of TiO_2 shift in the direction of low energy. The degree of shift varies with the different doping ions, which is consistent with the analysis result of band structure. For the N-doped TiO_2, a new peak appears above the valence band, and the width of the conduction band increases slightly. After codoping TiO_2 with N–A (A = Cr, Mn, Fe), the DOS peaks above the valence band and at the Fermi level are connected, thus expanding the width of the TiO_2 valence band. Therefore, the DOS peak above the valence band smoothens further, and a new DOS peak appears at the bottom of the conduction band. We can see that the width of the forbidden band of the codoped TiO_2 system (with the exception of N–V codoped TiO_2) is relatively less than that of pure and N-doped TiO_2.

We analyze the PDOS by comparing Figs. 4(a)–(g). In addition, we clarify the effect of single doping

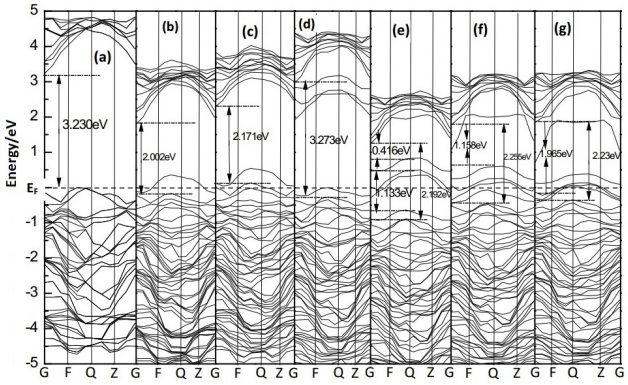

Fig. 2. Band structures of (a) pure, (b) N-doped, (c) N–Sc codoped, (d) N–V codoped, (e) N–Cr codoped, (f) N–Mn codoped, and (g) N–Fe codoped TiO_2.

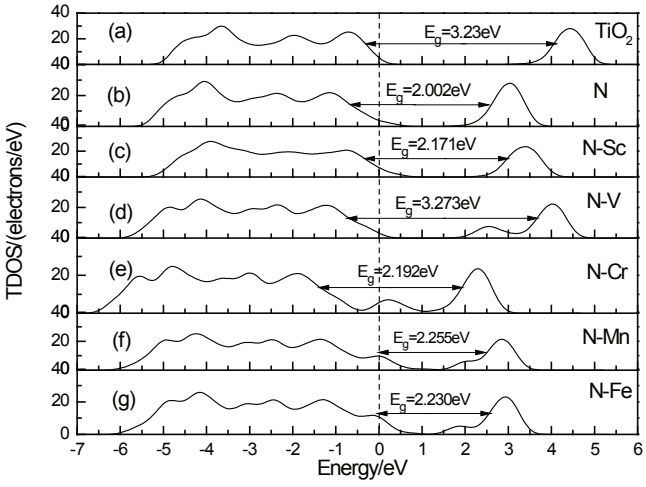

Fig. 3. Comparison of TDOS of (a) pure, (b) N-doped, (c) N–Sc codoped, (d) N–V codoped, (e) N–Cr codoped, (f) N–Mn codoped, and (g) N–Fe codoped TiO_2.

and codoping on the electronic properties of TiO_2. In N-doped TiO_2, an O atom is replaced by a N atom in the crystal lattice of TiO_2. Because there exists one more extranuclear electron of O atom than N atom, a hole defect is formed after doping. Therefore, the N-doped TiO_2 can be categorized as acceptor type doping[31]. TiO_2 is codoped with N–A (A = Sc, V, Cr, Mn, Fe), as shown in Figs. 4(c)–(g), some impurity levels are formed below the valence band and above the conduction band. After N–V codoping of TiO_2, a DOS peak A appears below the bottom of the conduction band because of V 3d or O 2p hybridization. However, the width of the forbidden band of TiO_2 increases slightly (Fig. 4(d)). After N–Cr codoping of TiO_2, the 2p orbital of O near the Fermi level and the t_{2g} orbital of Cr 3d are hybridized to form the DOS peak B (Fig. 4(e)). The hybrid impurity band is in the half-filled state. After the valence electrons absorb photons, they transit from the valence band to the impurity band and then to the conduction band. Therefore, the band gap reduces, which is in favor of the absorption of VIS light. After N–Mn or N–Fe codoping, N 2p and O 2p hybridize, resulting in the appearance of DOS peaks C or E above the valence band. Further, Mn t_{2g} or Fe t_{2g} and O 2p hybridize to form DOS peaks D or F that appear near the bottom of the conduction band. In addition, the DOS peaks C and D and E and F are connected. We can see that codoping alters the impurity state characteristics of N single-doped TiO_2. The continuous state, which is crosslinked by O 2p, N 2p, and (Mn, Fe) t_{2g}, is near the top of the valence band of TiO_2; therefore, it can significantly expand the valence band of the doped TiO_2. Further, codoping of TiO_2 with N–Mn or N–Fe can increase the degree of orbital hybridization of N 2p, O 2p and Ti 3d. Ti t_{2g} and O 2p of conduction band edge is divided; therefore, the covalent of N–Ti bond becomes stronger. The crosslinking of N 2p and Ti 3d in the valence band is enhanced, and the acceptor level near the top of valence band is closer to the valence band (compared with that of the N-doped TiO_2), thus forming a shallow acceptor level[32] which is beneficial to improve life of photon-generated carrier[33]. This improves the intensity of the impurity DOS near the top of the valence band and increases the probability of electron transition from the impurity energy level to the conduction band, which can enhance the utilization of solar energy. In addition, some electrons transition from the orbital of (Mn or Fe) 3d t_{2g} to the orbital of O 2p, which enhances the ionicity of the (Mn or Fe)–O bond. The results are consistent with the Mulliken population analysis. Moreover, there is a split between Ti t_{2g} and O 2p at the edge of the conduction

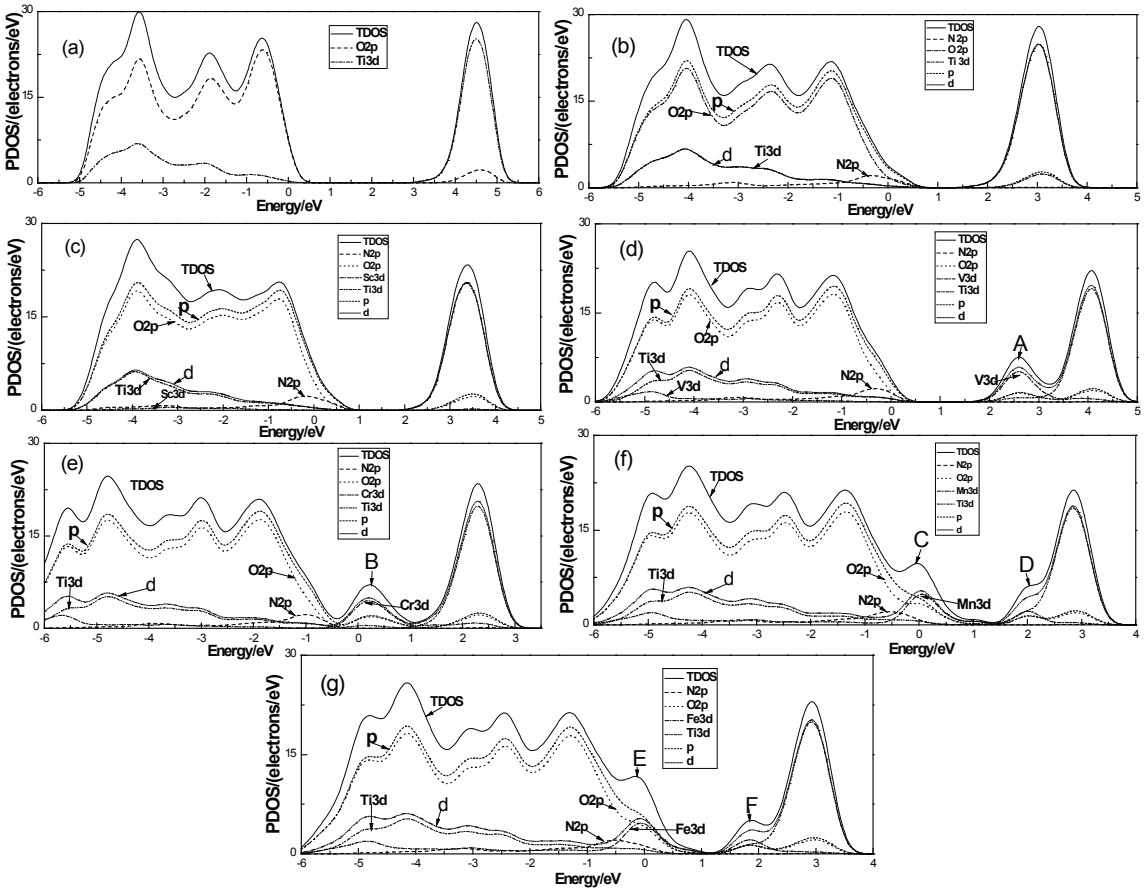

Fig. 4. Comparison of PDOS of (a) pure, (b) N-doped, (c) N-Sc codoped, (d) N-V codoped, (e) N-Cr codoped, (f) N-Mn codoped, and (g) N-Fe codoped TiO_2.

band. Part of the divided band is in the conduction band, and the others shift to a lower energy. In addition, the hybrid of (Mn or Fe)e_g near the bottom of the conduction band form new DOS peaks D or F. It can also enable the donor level near the bottom of the conduction band to shift closer to the conduction band and enhance the overlap with the conduction band, which forms a shallow donor level[32]. This is more likely to become the trap of photoproduction electrons[34]. It can effectively separate photoproduction electron–hole pairs and widen the conduction band, thus reducing the width of the forbidden band. Above all, the photocatalytic synergistic effect of N–Cr, N–Mn, and N–Fe is more evident than that of the others, which extends the lifetime of the photoproduction carrier, improves the reaction efficiency, and jointly promotes the photocatalytic activity of TiO_2 in the VIS region. The results are consistent with the previous analysis of the band structure.

The dielectric constant, absorption and reflection spectra of the pure, N-doped, and N–A (A = Sc, V, Cr, Mn, Fe) codoped TiO_2 are calculated with a scissors operator for correction. From the difference in the theoretical (2.134 eV) and experimental (3.23 eV) band gap values, the scissors operator is 1.096 eV.

The real and the imaginary parts of the dielectric function significantly affect the reflection and absorption of light. From the process of interaction between light and materials, the response of a material to light primarily involves two steps. First, when light shines on the surface of a material, the electrons in the valence band gain energy to enter the conduction band, and then the ground state is transformed into the excited state, which is the absorption of light. Second, in the excited state, the electrons are unstable and jump back to the lower energy level with the release of a photon or phonon, which is the reflection of material to light. The photon or phonon energy is equal to the energy difference between the excited state and the ground state. The collision between a phonon and the lattice is converted into heat energy[35]. Because we indicate the dissipation characteristics of the material to electromagnetic field with the imaginary part of the dielectric function, it directly affects the light absorption property of the material, namely, the greater the imaginary part, the greater the probability of photons absorption by electrons and the greater the number of electrons in the excited state. On the other hand, the real part of the dielectric function directly affects the light reflection property of the material, namely, the greater the real part, the greater the probability of emitted photons and the smaller the probability of generated phonons. Therefore, the imaginary and real parts of the dielectric function affect reflectivity similarly, namely, the greater the both parts, the higher the light reflectivity. The real and imaginary parts of the dielectric function of the pure, N-doped, and N–A (A = Sc, V, Cr, Mn, Fe) codoped TiO_2 are shown in Fig. 5.

From the vertical axis in Fig. 5, we can see that the imaginary and real parts of the dielectric function are clearly greater for the N–Fe, N–Cr, and N–Mn codoped TiO_2 than those of pure, N-doped, and N–Sc and N–V codoped. Therefore, the reflectivity of N–Fe, N–Cr, and N–Mn codoped TiO_2 is greater than that of the latter, and the reflectivity increases with increase in dielectric function.

We study the peak of the imaginary part, reflectivity, absorptivity, and the corresponding energy values of the pure, N-doped, and N–A (A = Sc, V, Cr, Mn, Fe). We analyze the effect of different types codoping on the optical properties (Table 2). Two peaks exist within the 0–10 eV range of the imaginary part of the dielectric function $\varepsilon_2(\omega)$ for the N–Sc, N–Cr, N–Mn, and N–Fe codoped TiO_2. The first peak of the imaginary part of N–Fe, N–Cr, and N–Mn codoped TiO_2 is significantly greater than that of the pure TiO_2, and the first peak of N–Fe codoped TiO_2 is the largest (Fig. 5). With respect to reflectivity and absorption within the range of 0–4 eV, the N–S, N–Cr, N–Mn, and N–Fe codoped TiO_2 have one peak, and the rest have no peaks. The peak values of reflectivity are approximately 0.219, 0.510, 0.348, and 0.646, respectively (Fig. 6). The peak values of absorptivity corresponding to the energies are approximately 2.205, 1.699, 2.196, and 1.947 eV, respectively (Fig. 7). The order of peak value is N–Fe > N–Cr > N–Mn > N–Sc. In conclusion, the relative reflectivity and absorptivity can be determined by quantitative comparison of the dielectric function imaginary part.

The reflection and optical absorption spectra of pure, N-doped TiO_2, and N–A (A = Sc, V, Cr, Mn, Fe) codoped TiO_2 are shown in Fig. 6 and Fig. 7, respectively. When compared with pure TiO_2, optical absorption increases in the VIS region for the different doping systems. When compared with N-doped

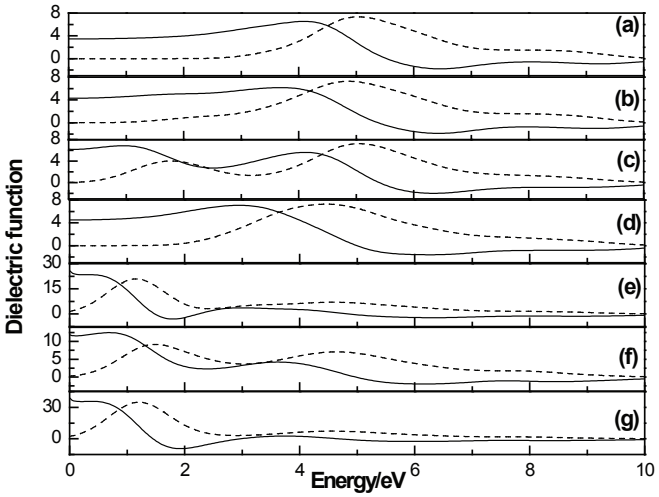

Fig. 5. Dielectric function of (a) pure, (b) N-doped, (c) N–Sc codoped, (d) N–V codoped, (e) N–Cr codoped, (f) N–Mn codoped, and (g) N–Fe codoped TiO_2.

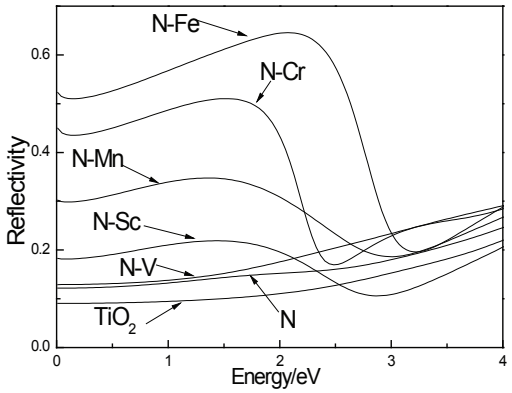

Fig. 6. Reflectivity of pure, N-doped, and N–A (A = Sc, V, Cr, Mn, Fe) codoped TiO_2.

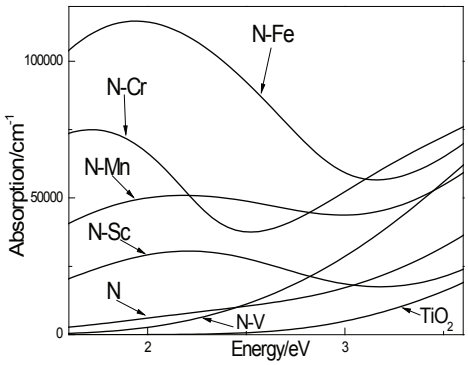

Fig. 7. Absorption spectra of pure, N-doped, and N–A (A = Sc, V, Cr, Mn, Fe) codoped TiO_2.

TiO_2, the width of the forbidden band gap of the N–A (A = Sc, V, Cr, Mn, Fe) codoped TiO_2 (except for N–V) is smaller, and the redshift is more apparent. From the analysis of energy level transitions, we can observe that a new impurity level is formed between the conduction and valence bands after N–A (A = Sc, Cr, Mn, Fe) codoping TiO_2 (except for N–V). This aids the transition of electrons from the impurity level above the valence band to the impurity energy level below the conduction band. Moreover, because the electronic DOS near the valence band increases significantly after N–A (A = Sc, r, Mn, Fe) codoping TiO_2 (except for N–V), the probability of electrons transfer from the impurity level to the conduction band and from the valence band to the impurity level below the conduction band can increase, thus improving the utilization of solar energy. The impurity level at the top of the valence band and near the bottom of the conduction band can effectively promote separation of photoproduction electron–hole pairs, thus improving the light quantum efficiency of TiO_2. Analysis of the effect of N–A (A = Sc, V, Cr, Mn, Fe) codoped TiO_2 on the atomic valence state electron shows that there is one more extranuclear electron of O atom than N atom. Therefore, the photoresponse

Table 2. Dielectric Function, Reflectivity, and Absorption Coefficient Peaks of Pure, N-doped, and N–A (A = Sc, V, Cr, Mn, Fe) codoped TiO_2.

Dopant Type	**Peak of Imaginary Part of Dielectric Constant**	**Energy corresponding to the Imaginary Part Peak of Dielectric Constant (eV)**	**Peak of Reflectivity**	**Energy corresponding to Peak of Reflectivity (eV)**	**Peak of Absorption Coefficient (cm^{-1})**	**Energy corresponding to Peak of Absorption Coefficient (eV)**
Pure TiO_2	7.336	5.035	None	None	None	None
N-doped TiO_2	7.278	4.866	None	None	None	None
N–Sc codoped TiO_2	4.027 7.247	1.797 5.058	0.219	1.421	3.057×10^4	2.205
N–V codoped TiO_2	7.273	4.455	None	None	None	None
N–Cr codoped TiO_2	20.913 6.999	1.149 4.605	0.510	1.502	7.495×10^4	1.699
N–Mn codoped TiO_2	9.178 7.068	1.478 4.632	0.348	1.353	5.093×10^4	2.196
N–Fe codoped TiO_2	34.859 7.287	1.197 4.572	0.646	2.072	1.147×10^5	1.947

range increases with the N-doped TiO_2. Further, the 3d orbital of Ti atoms contains only two d electrons. The 3d orbital electrons of Fe are the highest among those of A (A = Sc, V, Cr, Mn, Fe), and the d electron is more active than the s electron. Therefore, the absorption ability of N–Fe codoped TiO_2 in the VIS high-energy region is strong. Moreover, Cr and Mn contain the same number of d electrons (five). Because there is only one 4s orbital electron for Cr, which is in the half-filled state, it can easily become the electron trapping center by hybridization with p electron orbital. Therefore, the effect of N–Cr codoping is greater than that of N–Mn codoping.

We analyze the different doping systems by comparing Figs. (5)–(7). It can be found that the capacity of absorption and reflection of light in the VIS region does not increase with the doping atomic number, and the actual order is N–Fe > N–Cr > N–Mn > N–Sc > N–V > N.

In conclusion, the plane wave pseudopotential method based on the density functional theory is employed to study the band structure, DOS, and optical characteristics such as absorptivity, refractivity, and dielectric function of the N and transition metal (Sc, V, Cr, Mn, and Fe) codoped TiO_2. Analysis shows that the absorption and reflectivity of the doped system increase in the VIS region after N and N–A (A = Sc, V, Cr, Mn, and Fe) codoping TiO_2 and a codoping system is more outstanding compared with pure anatase TiO_2. In particular, from the comparison of the different doping systems band structures, the width of the forbidden band is shown to decrease in accordance with the band gap of N-doped TiO_2. Moreover, after N–A (A = Sc, Cr, Mn, Fe) codoping of TiO_2, the redshift becomes very obvious. The absorption and reflection capacities of light in the VIS region do not increase with the doping atomic number, with the actual order being N–Fe > N–Cr > N–Mn > N–Sc > N–V > N, because Fe has the largest number of 3d electron than other transition metals A (A = Sc, V, Cr, Mn, Fe), and d electron is more active than s electron. Therefore, the absorption ability of the N–Fe codoped TiO_2 is very high in the VIS high-energy region. However, the 4s atomic orbit of Cr is not completely filled, which hybridizes with the p electronic orbit to most probably act as photogenerated electron trap centers, resulting in the higher photocatalytic activity of N–Cr codoped TiO_2 when compared with N–Mn codoped TiO_2.

This work was supported by the National Natural Science Foundation of China (Nos. 61274128 and 61106129) and the Natural Science Foundation of Chongqing (No. CSTC2013JCYJA0731).

References

1. A. Fujishima and K. Honda, Nature **238,** 37 (1972).
2. M. H. Suhail, G. M. Rao, and S. Mohan, Appl. Phys. **71,** 1421 (1992).
3. M. R. Hoffmann, S. T. Martin, W. Y. Choi, and D. W. Bahnemann, Chem. Rev. **95,** 69 (1995).
4. T. H. Thanh, Q. V. Lam, T. H. Nguyen, and T. D. Huynh, Chin. Opt. Lett. **11,** 072501 (2013).
5. L. Yang, Y. Wang, and L. Zhao, Chin. Opt. Lett. **10,** 063102 (2012).
6. T. Harada, H. Murotani, S. Matumoto, and H. Honda, Chin. Opt. Lett. **11,** S10303 (2013).
7. H. H. Chen, F. Lei, J. T. Zhao, Y. Shi, and J. J. Xie, J. Mater. Res. **28,** 468 (2013).
8. S. Kimiagar and M. R. Mohammadizadeh, Eur. Phys. J. Appl. Phys. **61,** 10303 (2013).
9. R. Asahi, T. Morikawa, T. Ohwaki, K. Aoki, and Y. Taga, Science **293,** 269 (2001).
10. W. Choi, A. Termin, and M. R. Hoffmann, J. Phys. Chem. **98,** 13669 (1994).
11. T. Umebayashi, T. Yamaki, H. Itoh, and K. Asai, J. Phys. Chem. Soli. **63,** 1909 (2002).
12. Z. Y. Zhao, Q. J. Liu, J. Zhang, and Z. Q. Zhu, Acta Phys. Sin. **56,** 6592 (2007).
13. G. Kresse and J. Hafner, Phys. Rev. B **47,** 558 (1993).
14. J. P. Perdew, K. Burke, and M. Ernzerhof, Phys. Rev. Lett. **77**, 3865 (1996).
15. Z. Y. Yang, L.G. Peng, A. N. Zhou, and Y. P. Liu, New Chem. Mater. **34,** 35 (2006).
16. R. Asahi, Y. Taga, W. Mannstadt, and A. J. Freeman, Phys. Rev. B **61,** 7459 (2000).
17. C. Stampfl and C. G. Van de Walle, Phys. Rev. B **59,** 5521 (1999).
18. X. J. Zhang, Q. J. Liu, S. G. Deng, J. Chen, and P. Gao, Acta Phys. Sin. **60,** 087103 (2011).
19. R. Long and N. J. English, Appl. Phys. Lett. **94,** 132102 (2009).
20. R. Long and N. J. English, Chem. Lett. **22,** 1616 (2010).
21. R. Long and N. J. English, Phys. Rev. B **83,** 155209 (2011).
22. D. S. Huan, C. F. Chen, Y. H. Li, and R. J. Zeng, Chin. J. Inorg. Chem. **23,** 738 (2007).
23. X. C. Shen, *Semiconductor Spectrum and Optical Quality* (Science Press, Beijing, 1992).
24. V. M. Zainullina and V. P. Zhukov, Phys. Solid State **55,** 589 (2013).
25. P. Zhou, J. G. Yu, and Y. X. Wang, Appl. Catal. B **142,** 45 (2013).
26. Z. Y. Jiang, Y. M. Lin, T. Mei, X. Y. Hu, W. Z. Chen, R. N. Ji, E. Z. Liu, R. Z. Zhang, L. Zhang, Q. Zhang, B. Zhou, D. K. Zhang, J. Fan, H. Y. Zhu, X. D. Zhang, S. Z. Wan, S. S. Zhu, and Y. B. Shang, Comput. Mater. Sci. **68,** 234 (2013).
27. G. H. Wu, S. K. Zheng, P. F. Wu, J. Su, and L. Liu, Solid State Commun. **163,** 7 (2013).
28. H. X. Zhu and J. M. Liu, Comput. Mater. Sci. **85,** 164 (2014).
29. Y. Tian, Q. Feng, S. B. Din, T. Liu, J. M. Gao, and F. Wu, Acta Opt. Sin. **33,** 0816004 (2013)
30. K. N. Song, X. P. Han, and G. S. Shao, J. Alloys Compounds **551,** 118 (2013)
31. W. G. Zhu, X. F. Qiu, V. Iancu, X. Q. Chen, H. Pan, W. Wang, N. M. Dimitrijevic, T. Rajh, H. M. Meyer, M. P. Paranthaman, G. M. Stocks, H. H. Weitering, B. H. Gu, G. Eres, and Z. Y. Zhang, Phys. Rev. Lett. **103,** 226401 (2009).
32. X. G. Ma, L. Miao, S. W. Bie, and J. J. Jiang, Solid State Commun. **150,** 689 (2010).
33. Z. Y. Zhao and Q. J. Liu, Catal. Lett. **124,** 111 (2008).
34. L. C. Le, X. G. Ma, H. Tang, Y. Wang, X. Li, and J. J. Jiang, Acta Phys. Sin. **59,** 1314 (2010).
35. X. Q. He, D. J. Liu, Q. Duan, and Y. Zou, Laser J. **24,** 79 (2003).